Multispacecraft observations of a foreshock-induced magnetopause disturbance exhibiting distinct plasma flows and an intense density compression

D. L. Turner,[1,2,3] S. Eriksson,[3] T. D. Phan,[4] V. Angelopoulos,[5] W. Tu,[1,2,3] W. Liu,[2,3] X. Li,[1,2,3] W.-L. Teh,[3] J. P. McFadden,[4] and K.-H. Glassmeier[6,7]

Received 12 May 2010; revised 3 February 2011; accepted 8 February 2011; published 29 April 2011.

[1] Large-scale magnetopause disturbances can result from several different types of events, including those resulting from phenomena in the foreshock region. In this observational report, we present multipoint THEMIS observations of a magnetopause disturbance along the dawnside, equatorial flank that exhibits distinct flows in the magnetospheric plasma and an abnormally strong compression of the plasma density within it, which peaks at >7X the density of the near-Earth solar wind. We find that the fastest ion and electron flows are related to two different processes, the ion flows resulting from plasma being displaced around the disturbance and field-aligned electron flows, possibly related to magnetic reconnection. Interestingly, the magnetospheric plasma flows around the disturbance are very similar to those previously reported around flux transfer events, but we conclude that the disturbance is most likely the result of regions of compressed and rarified plasma density in the sheath resulting from a foreshock cavity. We present simple schematics of this foreshock cavity and its leading-edge compression region that explain many of the observed features and discuss possibilities for the intense density enhancement. Using the simultaneous THEMIS observations from the magnetosphere, magnetosheath, and solar wind, we propose that the abnormal density enhancement was the result of a combination of compression effects due to the magnetosheath and the cavity's leading-edge compression region coupled with some complex interaction near the magnetopause along the event's distinct boundary layer.

Citation: Turner, D. L., S. Eriksson, T. D. Phan, V. Angelopoulos, W. Tu, W. Liu, X. Li, W.-L. Teh, J. P. McFadden, and K.-H. Glassmeier (2011), Multispacecraft observations of a foreshock-induced magnetopause disturbance exhibiting distinct plasma flows and an intense density compression, *J. Geophys. Res.*, *116*, A04230, doi:10.1029/2010JA015668.

1. Introduction

[2] Several types of transient events that occur near or at the magnetopause can result in large-scale magnetopause deformation. Such events are important to solar wind-magnetosphere interactions because they can result in plasma mixing between the magnetosheath and the magnetosphere. Magnetopause disturbances can result from any of several different phenomena such as flux transfer events (FTEs) [e.g., *Owen et al.*, 2008], Kelvin-Helmholtz (KH) surface waves and vortices [e.g., *Hasegawa et al.*, 2004], foreshock cavities [e.g., *Sibeck et al.*, 2002], hot flow anomalies (HFAs) [e.g., *Jacobsen et al.*, 2009], and solar wind pressure pulses [e.g., *Sibeck*, 1990]. Of these, foreshock cavities and HFAs are phenomena originating in the foreshock region, yet it can be difficult to determine the causes of magnetopause disturbances due to the ambiguity in various observations of these different phenomena. This ambiguity can arise from similar features in the different phenomena, a lack of multipoint measurements, and/or a lack of near-Earth solar wind or magnetosheath measurements. In this work, we analyze detailed, multipoint observations of an interesting magnetopause disturbance observed on 21 November 2008 that displays an abnormal compression of plasma density, and we show that the disturbance is most likely the result of dynamics related to foreshock phenomena.

[3] The foreshock is the region upstream of Earth's bow shock characterized by particles flowing upstream from the shock (i.e., backstreaming) along the interplanetary magnetic field (IMF) lines that intersect it. Foreshock cavities result from kinetic interactions between foreshock and

[1]Department of Aerospace Engineering Sciences, University of Colorado at Boulder, Boulder, Colorado, USA.
[2]Laboratory for Space Weather, Chinese Academy of Sciences, Beijing, China.
[3]Laboratory for Atmospheric and Space Physics, University of Colorado at Boulder, Boulder, Colorado, USA.
[4]Space Sciences Laboratory, University of California, Berkeley, California, USA.
[5]Department of Earth and Space Sciences, University of California, Los Angeles, California, USA.
[6]Institut für Geophysik and Extraterrestrische Physik, Technische Universität Braunschweig, Braunschweig, Germany.
[7]Max Planck Institute for Solar System Research, Katlenburg-Lindau, Germany.

0148-0227/11/2010JA015668

solar wind plasmas [e.g., *Sibeck et al.*, 2002]. Near the bow shock, these cavities of depressed density and field strength, which result from expanding regions containing enhanced fluxes of suprathermal ions backstreaming along field lines connected to the bow shock, can form between regions of field lines that are disconnected from the bow shock. In such cases, kinetic interactions result in the solar wind upstream of the bow shock being modified such that it produces crater like features in the total magnetic field strength and number density as the regions on either side of the expanding, lower-density cavity undergo compression. *Thomas and Brecht* [1988] presented a model consistent with this in which hybrid simulations were used to demonstrate how a beam of backstreaming ions could produce such features in solar wind plasma. Foreshock cavities are not uncommon features, which was a result demonstrated by *Sibeck et al.* [2001], who conducted a study of the foreshock using IMP 8 data from January to August 1995 and found 292 foreshock cavities during this period. Foreshock cavities need not be associated with IMF discontinuities [*Sibeck et al.*, 2002], though such IMF variations can transport a foreshock cavity past a spacecraft [e.g., *Sibeck et al.*, 2000].

[4] Upstream of the bow shock, the features associated with foreshock cavities diminish rapidly [*Sibeck et al.*, 2004]. However, *Fairfield et al.* [1990] presented observational evidence that pressure changes in the solar wind resulting from the foreshock (e.g., foreshock cavities) can propagate through the bow shock and magnetosheath and impinge on the magnetopause. Similar to solar wind dynamic pressure variations (discussed below), the pressure variations generated by a foreshock cavity result in magnetopause motion, either inward or outward depending on the variation, to maintain the pressure balance at the boundary [e.g., *Sibeck et al.*, 2000]. The features generated by such pressure variations and consequent magnetopause motion would be similar to those described for solar wind pressure variations, which may have been mistaken previously for features associated with FTEs [*Sibeck*, 1992], yet the motion would have distinct characteristics based on the different regions of the foreshock cavity (i.e., the compressed leading and trailing edge regions and the central, low-density region).

[5] More extreme than foreshock cavities, yet similar to them in the way they form, are HFAs, which were first discussed by *Schwartz et al.* [1985] and *Thomsen et al.* [1986]. They are associated with discontinuities in the IMF, and when HFA features propagate through the magnetosheath and encounter the magnetosphere, they can result in large-scale motion of the magnetopause. For example, *Jacobsen et al.* [2009] presented an observational report of a HFA on 30 October 2007 that resulted in a very large magnetopause deformation in which the magnetopause moved outward by close to 5 R_E in just under 1 min. HFAs contain hot plasma (10^6–10^7 K) in their central regions, which also have disturbed magnetic fields, ion flux enhancements in the keV energy range, significant dynamic pressure dropouts, and densities the same as or lower than that of the surrounding solar wind [*Schwartz et al.*, 1985; *Thomsen et al.*, 1986]. These disturbances move along the magnetopause as the IMF current sheet passes over the magnetosphere, and to a spacecraft near the magnetopause, the resulting observations can closely resemble a FTE. HFAs are also very similar to foreshock cavities, but HFAs and foreshock cavities differ in that HFAs result in large reductions or deflections of plasma flow velocities through the events, nearly isotropic and Maxwellian distributions through the events, and large ion temperature variations [*Thomsen et al.*, 1986; *Sibeck et al.*, 2002]. For a HFA to form, one critical condition is that the convection electric field on at least one side of the IMF discontinuity should be pointing toward the discontinuity to drive reflected ions into it [*Thomsen et al.*, 1993]. *Facsko et al.* [2008] conducted a statistical study of 33 HFAs, and they found much evidence supporting some previously recognized formation conditions and characteristic features required for HFAs. The characteristic features included (1) a crater-like feature in the magnetic field strength with sharp edges compared to the nonperturbed solar wind on either side of it, (2) a drop in the solar wind speed with a velocity turned away from the Sun-Earth line, (3) an increase in temperature up to several 10s of millions of Kelvin, (4) a crater-like feature in the solar wind number density. They also proposed a new formation condition for HFAs, namely that fast solar wind is essential to HFA formation.

[6] In this paper, we present observations of an abnormally strong compression of the plasma density during a large-scale magnetopause disturbance that occurred on 21 November 2008. We begin by discussing the data sets employed and observations of the event. Solar wind measurements at Earth are available for this event from THEMIS-B (TH-B), and the magnetopause disturbance itself is observed by three of the other THEMIS spacecraft, TH-A, -D, and -E, which are distributed along the dawn flank of the magnetopause at the time of the event. There is evidence against the event resulting from KH vortices or a FTE. We also present evidence that the event is most likely not the result of a pressure pulse in the solar wind or a hot flow anomaly, and we show that the observations are most consistent with a foreshock cavity. We provide an analysis of the various features associated with this magnetopause disturbance, including its scale size, the plasma distributions of the fast flows around it, and the pressure balance throughout it. In the discussion, we speculate on the cause of the abnormally strong density enhancement observed during this event and present some interesting questions. Overall, the THEMIS multipoint measurements of this foreshock cavity provide detailed observations of (1) the foreshock cavity in the solar wind just upstream of the bow shock, (2) its effect in the magnetosphere near the magnetopause, and (3) some of its properties in the magnetosheath including the abnormal compression of plasma density along the event's boundary.

2. Observations

[7] Launched on 17 February 2007, the Time History of Events and Macroscale Interactions during Substorms (THEMIS) mission consists of an extensive network of ground-based instruments and five small, identical spacecraft [*Angelopoulos*, 2008]. In 2008, these spacecraft were in a set of orbits with different altitudes at apogee ranging from 10 to 30 R_E, and throughout the year, these orbits allowed the spacecraft to sample a massive range of Earth's magnetosphere, magnetosheath, and the near-Earth solar wind. On 21 November 2008, the THEMIS constellation had apogees on Earth's dawnside. Figure 1 shows the locations of the

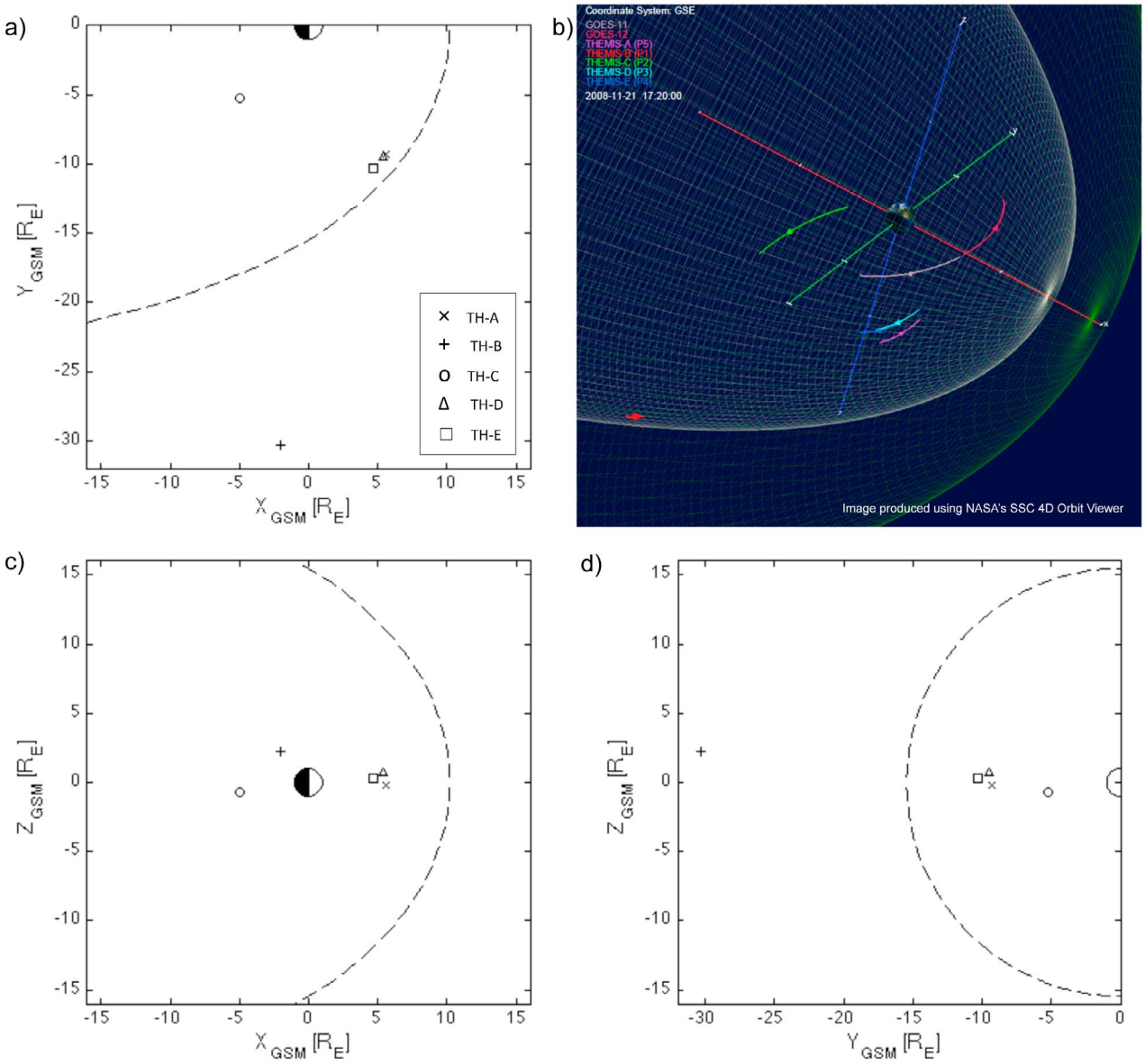

Figure 1. (a, c, and d) TH-A (cross), TH-B (plus), TH-C (open circle), TH-D (triangle), and TH-E (square) GSM locations at 1720 UT with the *Shue et al.* [1997] magnetopause shown where it intersects each plane (dashed line). (b) Three-dimensional orbit view in GSE coordinates of the THEMIS and GOES spacecraft at 1720 UT with orbital tracks for ±2 h. Model magnetopause and bow shock are also shown as wireframes.

five THEMIS spacecraft at 1720 UT, just before three of the probes observe a disturbance near the magnetopause. The intersection of the *Shue et al.* [1997] magnetopause, calculated using the TH-B solar wind conditions at 1720 UT, with each plane is shown with the dashed lines. TH-A, TH-D, and TH-E are located around 0800 MLT near the magnetopause, and they all observe the disturbance. As can be seen in Figure 1, TH-A and TH-D straddle the magnetic equator close to the same distance in X_{GSM}, while TH-E is within 0.3 R_E of the magnetic equator and slightly further downtail. TH-C is still in the inner magnetosphere and is not used in this study. Finally, TH-B is near the dawn-dusk meridian and well outside of the magnetopause.

[8] Figure 2 shows fluxgate magnetometer [*Auster et al.*, 2008] and electrostatic analyzer (ESA) [*McFadden et al.*, 2008] data from the three THEMIS spacecraft that observe the disturbance: TH-A, TH-D, and TH-E. Magnetic fields and velocities here show the magnitudes (black) and components (colors) in LMN coordinates, in which N is the magnetopause normal direction (positive outward), M lies in the equatorial plane, and L completes the right-handed coordinate system [*Russell and Elphic*, 1978]. Using this LMN, boundary-normal coordinate system, on the dawnside (duskside) of the equatorial magnetopause, the M-direction has an antisunward (sunward) component, with the L-direction primarily in the expected direction of the field just inside the

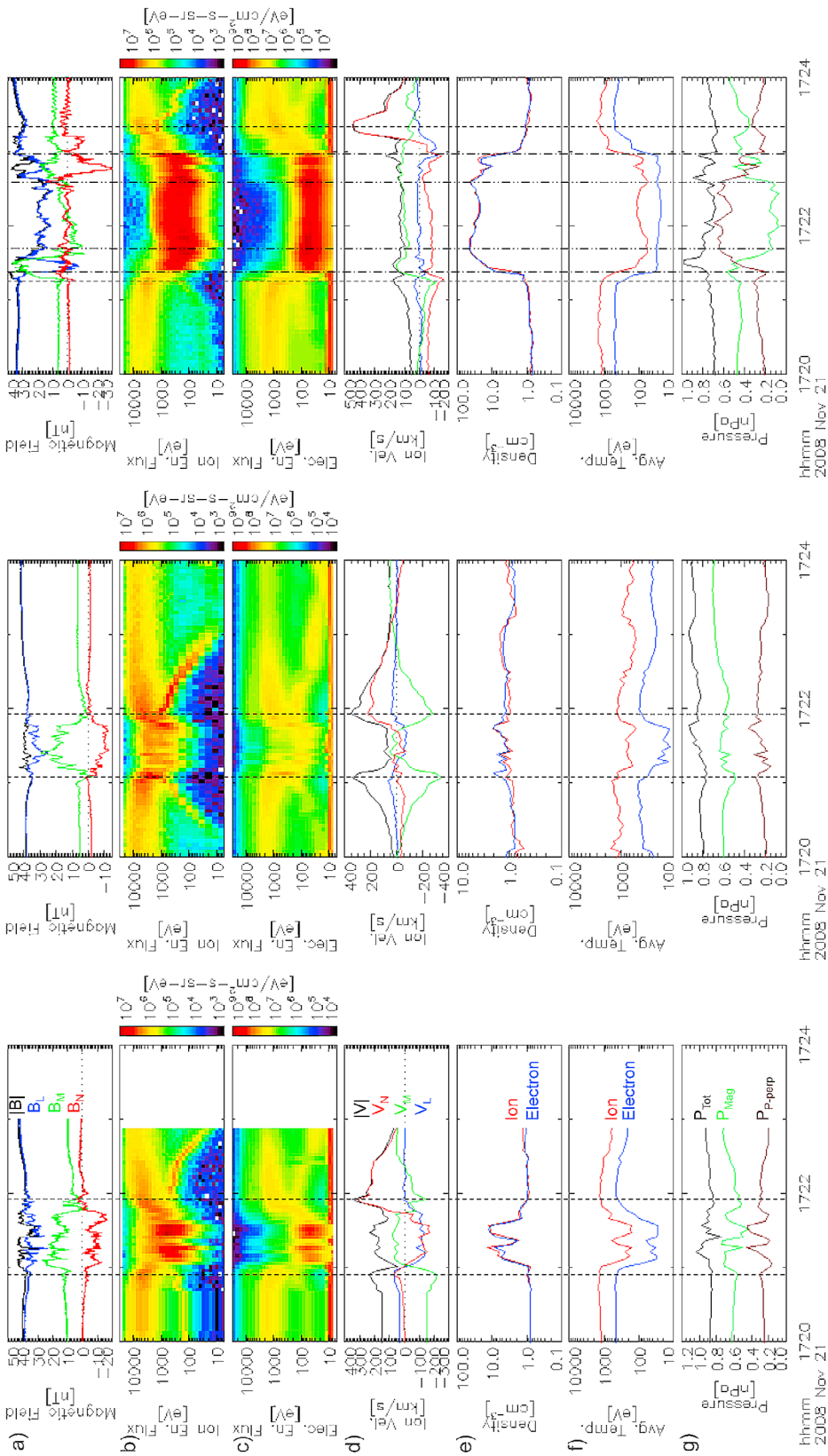

Figure 2. (left) TH-A, (middle) TH-D, and (right) TH-E observations. The (a) total magnetic field and the field components in LMN, (b) ion and (c) electron energy-time flux spectrograms, (d) ion total velocity and components in LMN coordinates, (e) plasma density and (f) average temperature, and (g) calculated pressures are shown. TH-A observations are cut short due to the end of burst-mode data. Various dashed vertical lines are used for reference and are described in the text.

magnetosphere. The LMN components displayed in Figure 2 are calculated based on a statistical magnetopause [i.e., *Fairfield*, 1971]. These directions are dependent on each spacecraft's location and are continually changing, but for a sense of their values in GSM around the time of the event, the following equation converts from GSM to LMN for TH-E's location at 1720:02 UT:

$$\begin{bmatrix} L \\ M \\ N \end{bmatrix} = \begin{bmatrix} -0.0149 & 0.0145 & 0.9998 \\ -0.6991 & -0.7150 & 0.0000 \\ 0.7149 & -0.6989 & 0.0208 \end{bmatrix} \cdot \begin{bmatrix} X \\ Y \\ Z \end{bmatrix}_{GSM} \quad (1)$$

The magnetopause disturbance in question here is first observed by TH-A and -D at around 1720:55 and 1721:05 UT, respectively, based on the initial peaks in ion velocity (marked on Figure 2 with the vertical dashed lines) and then later by TH-E at 1721:16 UT. In Figure 2, the data from each of the three spacecraft are displayed in the columns from left to right. For each of the spacecraft in Figure 2, the highest resolution data available are shown for 1720–1724 UT, when the disturbance is observed. The effects of the event itself are clearly visible in Figure 2 as the large disturbance in all of the data. Prior to the disturbance, conditions are calm and as expected for the near-magnetopause magnetosphere. The magnetic field is primarily in the L-direction as observed by all three spacecraft, and the magnitude of the field ranges from ~35 nT (TH-E) to ~40 nT (TH-A and -D), which also confirms that TH-E is closest to the magnetopause. When the event is observed, TH-A and TH-D observe weaker B_L and enhancements in B_M and B_N. TH-A observes a significant, double-peaked enhancement of plasma density up to ~10 cm^{-3}, while TH-D observes less of a change in the plasma density. The average ion and electron temperatures are inversely correlated with the densities. Both spacecraft also observe dropouts in the more energetic fluxes and enhancements of lower-energy fluxes for both ions and electrons. One of the clearest features in the TH-A and -D observations are the fast ion flows (in V_M and/or V_N) that flank the features of the main disturbance (i.e., those associated with the enhancements in B_M and low-energy flux). Similar, several hundred km/s flows are also seen in the electron velocities, though these are not shown in Figure 2. Associated with these ion flows are lower-energy flux enhancements visible in the energy-time spectrograms, which we will discuss later in this paper, and are referred to throughout as "wings" in the flux spectrums. TH-A observes a weak-positive to negative to strong-positive turnover in V_N with an opposite tripolar signature in V_M, revealing increased negative flows on either side of the disturbance and a positive V_M through the center of the encounter. V_L reveals strong negative flows through the center of the encounter. TH-D observes very similar features, though the total velocity associated with the center of the encounter is not as fast as that observed by TH-A, and the strong negative V_M flows flanking the disturbance are the dominant features observed by TH-D. TH-D also observes weak V_N at the start of the encounter and strong V_N at the end, which is also similar to TH-A. The maximum total velocities observed by TH-A and -D are between 300 and 400 km/s, and the times these occur are indicated with the dashed vertical lines for all three spacecraft.

[9] TH-E observes a longer encounter with the event and many of the features observed by this spacecraft are more extreme than those observed by TH-A and -D. During the main part of the disturbance, as seen in Figure 2, TH-E observes crater-like features in total magnetic field strength, with a strong overall dropout through the center of the encounter and enhanced total strength observed at the edges of this dropout. Strong positive B_M enhancements and dropouts in B_L are also seen on either edge of the center of the encounter, and on the trailing edge, B_N becomes strongly negative. Through the center of the encounter (i.e., the period occurring between the vertical dash-dot-dotted lines), B_M undergoes a clear negative-to-positive turnover, while B_L is the dominant component. The density enhancement observed by TH-E occurs within the times marked by the vertical dash-dotted lines. This enhancement is very strong, going from normal magnetospheric levels of less than 1 cm^{-3} to a peak value of over 44 cm^{-3} through this portion of the encounter. A strong drop in ion temperature is also clearly visible through this portion of the encounter. The associated dropouts in the energetic ion and electron fluxes and enhancements in the low-energy fluxes are more clear than those observed by TH-A and -D, though the observations of the plasma "wings" on the flanks of the encounter are not as clear. Finally, the velocities observed by TH-E are faster upon exiting the disturbance than upon entering it, and the maximum velocity gets up to ~450 km/s and is primarily in the positive N-direction.

[10] Examining the data after the initial disturbance, there are some additional features that should be noted in the TH-E observations. Figure 3 shows TH-E magnetic fields, ion quantities, and pressures for the 10-min period from 1720 to 1730 UT. Note that after the initial disturbance is first observed from ~1721:20 to 1723:30 UT, the magnetic field strength undergoes an overall enhancement followed by another decrease before returning to approximately its preevent level just shortly after 1728 UT. Associated with these magnetic field features are ion flux enhancements, including another feature that is similar to the "wings" seen before, enhanced velocities, and variations in the magnetic and plasma pressures. Note that at around 1724:25 UT, V_N changes from positive to negative. In the next section, we will analyze these particular features as well as those mentioned above from all three spacecraft to provide evidence concerning the underlying nature of this event.

[11] Figure 4 shows data from the magnetic field and plasma instruments on TH-B from 1705 to 1735 UT. From the strength and components (in GSM) of the magnetic field and the plasma energy fluxes and density, it is clear that TH-B is in the solar wind. Note here that the density plot includes WIND-SWE ion densities (with times adjusted by 89 min from ballistic propagation to account for the offset from WIND being upstream in the solar wind) and that the TH-B ion density has been corrected based on the electron density since the ESA instrument was taking solar wind measurements while still in magnetosphere mode and cannot necessarily resolve the narrow solar wind beam. For this correction, the ion densities are simply multiplied by 1.62, which is the ratio of the average electron to ion densities during this 30-min period. Under these conditions, the electron density is more accurate than that for the ions [see *McFadden et al.*, 2008]. It should also be noted that the magnitude of the ion temperature is unreliable, and the velocity directions (V_Y and V_Z) may be inaccurate (though

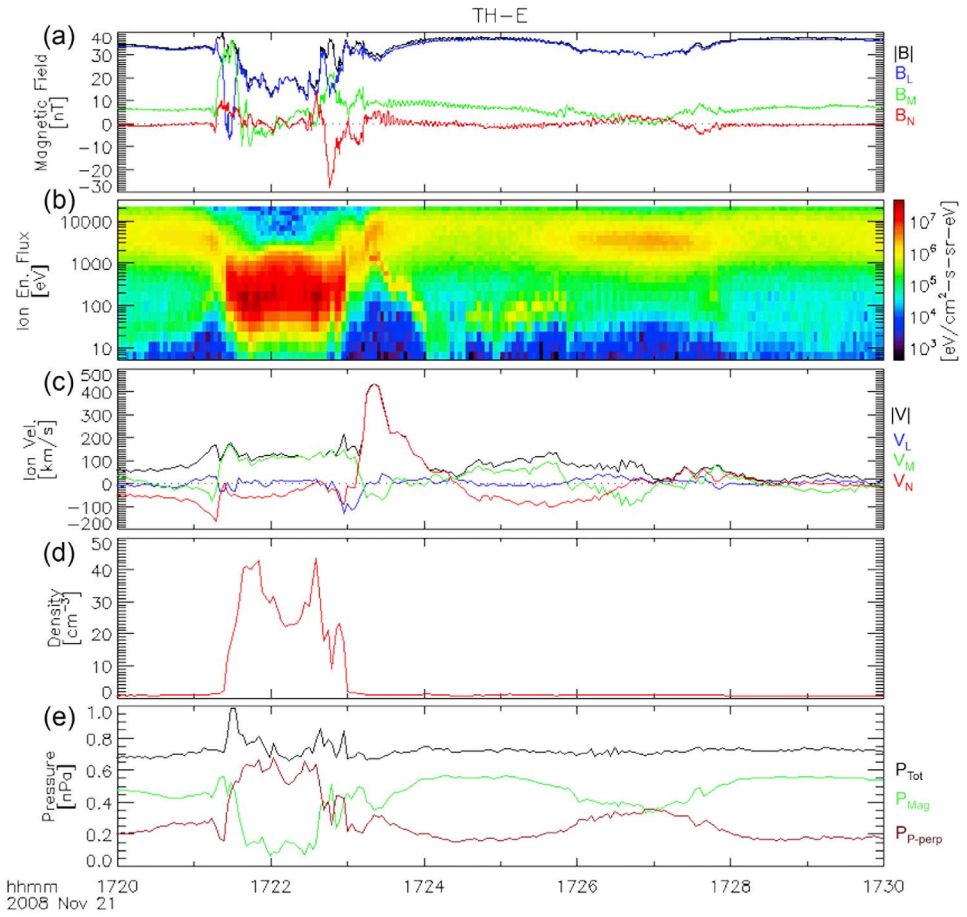

Figure 3. TH-E observations from 1720 to 1730 UT. (a) Magnetic field and velocity components are shown in LMN coordinates, and the line colors all correspond to those from Figure 2. For the plasma quantities (i.e., (b) ion energy fluxes, (c) ion velocity, and (d) density), reduced resolution data are shown. Note also that the density plot scale is linear, unlike in Figure 2. (e) The total, magnetic, and perpendicular plasma pressures are shown.

the magnitude is accurate). Conditions are generally calm prior to the abrupt dawnward turning of the IMF B_Y at ~1719:30 UT. This IMF turning apparently sets the appropriate conditions to put TH-B into the foreshock region from ~1719:30 to 1730:20 UT, and starting from shortly after 1721 UT, TH-B observes suprathermal ions and depressed plasma density and dynamic pressure, which are characteristics of the foreshock. Another IMF discontinuity at ~1730 UT apparently changes the conditions such that TH-B is no longer in the foreshock. Upon exiting the foreshock region, TH-B observes crater-like features in the total field strength, density, and dynamic pressure from ~1728 to 1731 UT, before they return to levels observed earlier in the solar wind. Note also that the IMF B_Z is primarily southward prior to the discontinuity at ~1730 UT and northward after it.

3. Analysis and Interpretation

3.1. Event Classification

3.1.1. Evidence for a Foreshock Cavity

[12] A foreshock cavity in the solar wind consists of a central region of depressed field strengths and plasma density flanked on either side by compressed regions with enhanced fields and density, which result in crater-like features in these quantities as observed by a spacecraft passing through them. The features observed by TH-B on 21 November 2008 are consistent with this. TH-B is apparently in the foreshock from shortly after 1721 UT until the IMF discontinuity at ~1730 UT. Associated with this discontinuity are crater-like signatures in the total field strength, density, and dynamic pressure from ~1728 to 1731 UT, which are highly consistent with previous observations [e.g., *Sibeck et al.*, 2002; *Schwartz et al.*, 2006; *Billingham et al.*, 2008] and simulations [e.g., *Thomas and Brecht*, 1988] of foreshock cavities upstream of the bow shock. The pressure variations associated with the different regions of a foreshock cavity can propagate through the magnetosheath and result in a disturbance along the magnetopause [*Sibeck et al.*, 2000], and ground magnetometer observations from the THEMIS network of stations reveal some very clear magnetic impulse events (MIEs). These signatures (not shown here; see Inuvik and Bettles stations during this event for clear examples) have been used previously to identify magnetopause motion resulting from pressure variations in the sheath [e.g., *Sibeck et al.*, 1989].

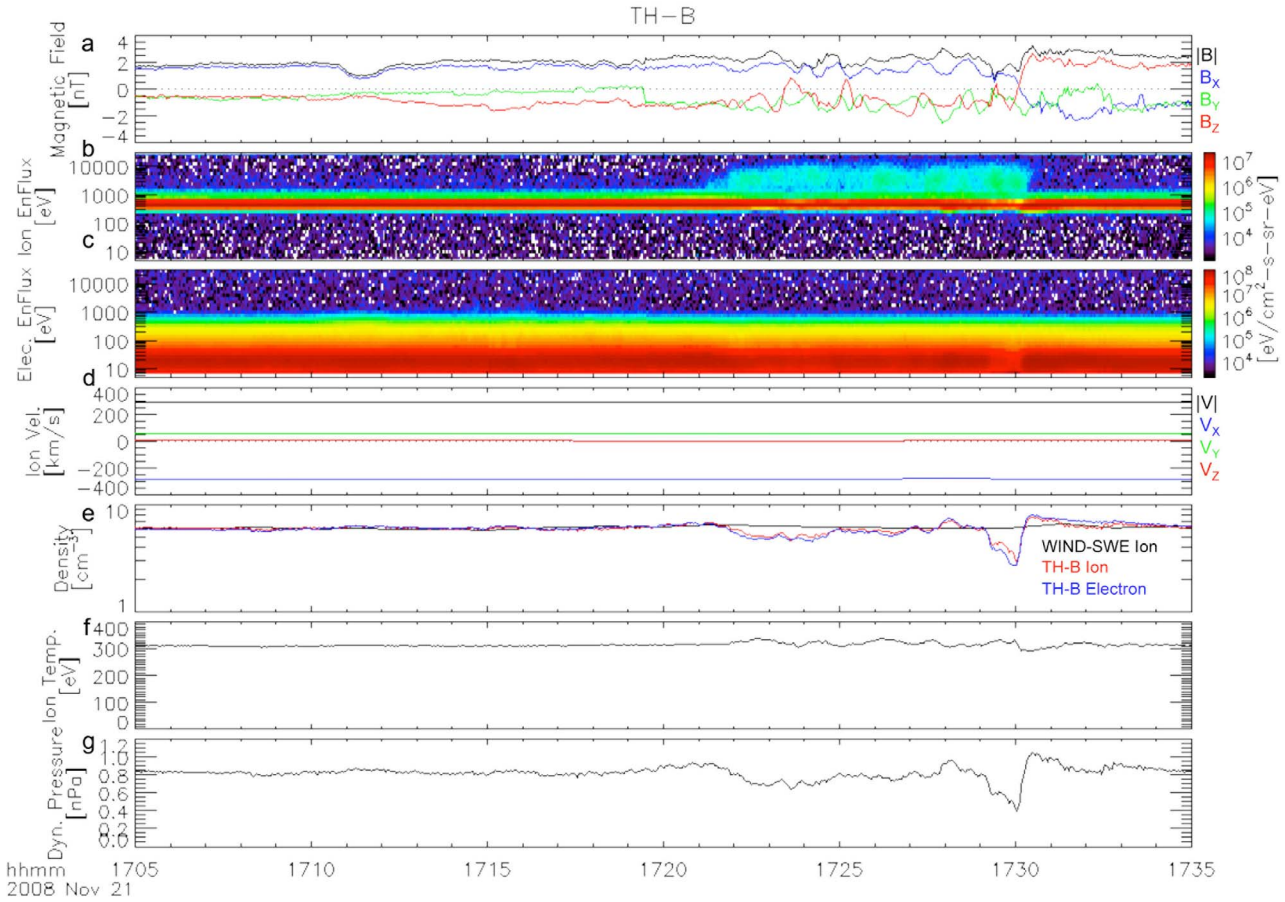

Figure 4. TH-B observations: magnetic field and velocity components are in GSM with X_{GSM} in blue, Y_{GSM} in green, and Z_{GSM} in red, with the magnitude displayed in black. (a–g) Same format as in Figures 2a–2g except the Figure 4g displays dynamic pressure only. WIND ion densities from the SWE instrument are also shown in black in Figure 4e.

[13] From ~1721 to 1728 UT, TH-E also observes (refer to Figure 3) different regions, possibly related to a foreshock cavity. During the initial disturbance, the magnetopause moves inward toward TH-E, as indicated by the negative V_N, and apparently it actually passes over the spacecraft from 1721:25 to 1723:00 UT, leaving it in the sheath during this period. Next, from ~1723 to 1726 UT, TH-E returns to the magnetosphere and observes fields and plasma that are similar to those before and after the event. When TH-E first reenters the magnetosphere, it observes very fast outward motion in the normal direction. Then around 1724:25 UT, V_N flips from positive (i.e., outward) to negative (inward), which indicates that the magnetopause is moving back in toward TH-E. From ~1726 to 1728, TH-E is apparently closer to the magnetopause again, observing very similar field, flux, and pressure features to those observed around 1723:20 UT when it was near the magnetopause. Summarizing these TH-E observations, the magnetopause first moves inward (and over) the spacecraft, and then it passes back over and away from the spacecraft before moving in toward it again and finally settling back to its preevent configuration. This is consistent with how the magnetopause should behave as a foreshock cavity passes over it; the leading and trailing compressed regions result in inward magnetopause motion, while the rarified central region results in outward motion. In the solar wind, TH-B observes a much shorter encounter. The crater-like features it observes are consistent with a foreshock cavity passing by in the solar wind near the bow shock, the intensity of which should be diminished compared to an observation of the same event in the sheath [*Sibeck et al.*, 2004].

[14] Figure 5 is a sketch displaying the scenario in which a foreshock cavity moves along the magnetopause with the IMF discontinuity that was observed by TH-B at ~1730 UT. Using the TH-B data, a minimum variance analysis (MVA) [e.g., *Sonnerup and Scheible*, 1998] is employed during 1729:36–1731:00 UT to determine the orientation of the IMF discontinuity, which reveals a discontinuity normal direction with XYZ_{GSM} coordinates of (−0.7976, −0.2661, −0.5412) R_E. The normal direction is well defined based on this MVA, with an intermediate to minimum eigenvalue ratio of 9.4. Assuming propagation at ~205 km/s, which is the component of the solar wind speed along the discontinuity normal direction, with a separation between TH-E and TH-B along this normal direction of 9.8 R_E, the discontinuity would take only around 5 min to travel from TH-E to TH-B. Next, if we assume that the foreshock cavity is approximately symmetric about the IMF current sheet, which is also consistent

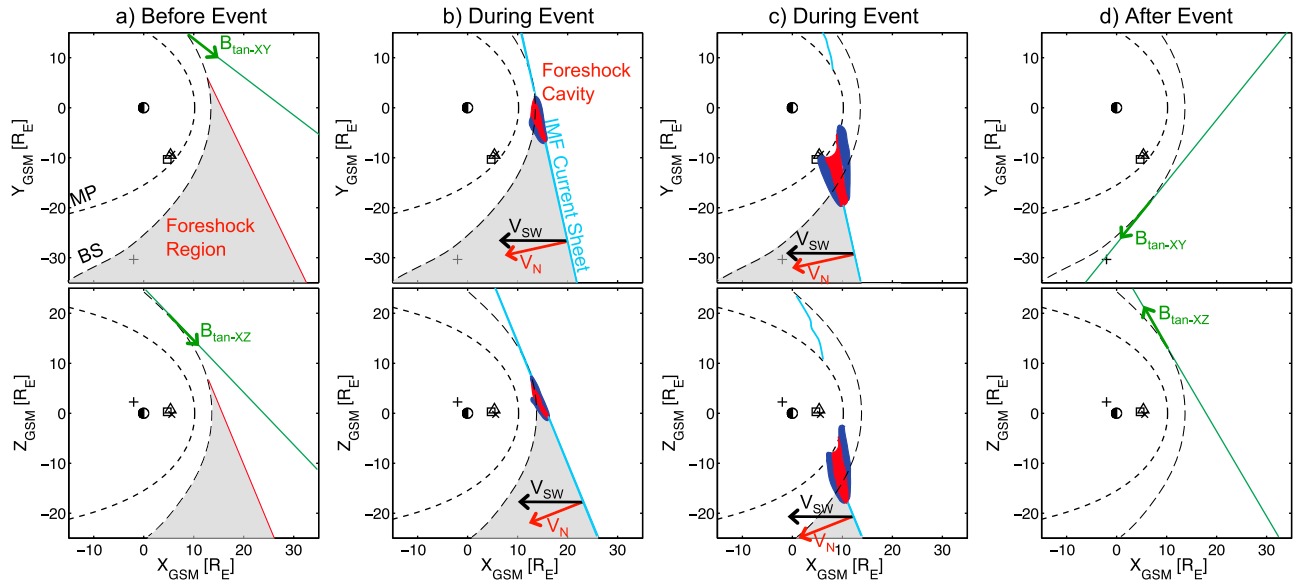

Figure 5. Sketch depicting the passage of the current sheet in the IMF observed by TH-B at ~1730 UT. Cross-sections in the XY and XZ GSM planes are shown for four different times: (a) before the event is observed, with the preevent tangential IMF shown and an estimated foreshock region (shaded gray); (b) when the IMF discontinuity (blue line marked "IMF current sheet") first impacts the bow shock, possibly triggering a foreshock cavity (red shaded region with the compressed regions on the flanks represented with dark blue shading); (c) around the time when the event is initially observed at TH-A, TH-D, and TH-E, with the effects of the foreshock cavity having propagated through the magnetosheath; and (d) after the discontinuity has passed leaving behind it a new orientation of the IMF.

with a similar scenario presented by *Sibeck et al.* [2000], then we can approximate whether the timing in the observations is consistent with a foreshock cavity moving with the IMF discontinuity. TH-E encounters the effects of the apparent foreshock cavity centered around ~1724:25 UT, corresponding to the turnover in V_N and around the time of the local maximum in total field strength. Meanwhile, TH-B encounters the center of the cavity around 1729:45 UT, which is a difference of just over 5 min. Thus the IMF discontinuity could indeed be responsible for moving a foreshock cavity past TH-A, TH-D, and TH-E along the magnetopause.

[15] We can also estimate a scale size of the initial compression region in the direction of its motion along the magnetopause by taking into account the spacecraft separations at a time when all three spacecraft observe the event simultaneously. At 1721:30 UT, all three spacecraft observe the initial compression, with TH-A and TH-D near the end of their encounters and TH-E at the beginning of its encounter. At this time in the M-direction, 0.2 R_E separates TH-A and TH-D, 0.7 R_E separates TH-A and TH-E, and 0.5 R_E separates TH-D and TH-E. This reveals that the scale size of this cross-section of the initial compression region is ~1 R_E. As observed by TH-E, the entire event takes just under 7 min to pass by at the slowed magnetosheath speed, which we can approximate with the speed observed within the initial disturbance by TH-E (i.e., ~125 km/s). This reveals a scale size of ~8 R_E for the foreshock cavity event in its velocity direction along the magnetopause as observed by TH-E. Finally, in the solar wind as observed by TH-B, the event takes just over 3 min to pass by based on the crater signatures in B_{Tot}, density, and pressure. Given the solar wind speed of ~300 km/s, this also reveals a scale size of ~8 R_E in the velocity direction.

3.1.2. Evidence Against Other Phenomena

3.1.2.1. FTE or KHI

[16] Though TH-E does observe crater-like features in B_{Tot} during the initial disturbance there is no continuous bipolar signature in B_N, which is evidence against a FTE. Also, a FTE alone cannot explain the in-out-in magnetopause motion observed by TH-E between 1721 and 1728. Being near ~0800 MLT on the dawn side of the magnetopause, it is unlikely that a full KH vortex would have formed [e.g., *Otto and Fairfield*, 2000]. Additionally, when TH-E crosses into the center of the initial disturbance, it observes magnetosheath-like plasma with no indication of magnetospheric plasma mixed in it. Primarily for these reasons, we do not believe that the disturbance in question was the result of a FTE or the KH instability, neither of which can also explain the crater-like features observed by TH-B between ~1728 and 1731 UT.

3.1.2.2. Solar Wind Pressure Pulse

[17] The magnetopause is the boundary where the magnetic pressure from Earth's magnetic field balances the dynamic pressure of the solar wind, and thus variations in the solar wind dynamic pressure result in variations on the magnetopause. WIND-SWE data are available at the time of this event (courtesy of R. Lin of UC-Berkeley and K. Ogilvie of NASA-GSFC and NASA's CDAWeb online database). They are consistent with the TH-B solar wind measurements and confirm that the solar wind density and velocity show no signs of a dynamic pressure pulse that would result in a

significant compression of the magnetosphere. It should be noted here that we have greater confidence in the adjusted TH-B ion density measurements based on their good agreement with the WIND ion densities as is shown in Figure 4. Magnetic fields measured at geosynchronous orbit by the GOES-11 and GOES-12 spacecraft (not shown; courtesy of H. Singer of NOAA-SWPC and NASA's CDAWeb) further confirm this, as they are both on the dayside at ~0900 and ~1300 MLT, respectively, and reveal no clear signs of a field compression at the time of the event. However, both GOES spacecraft do observe what appear to be ULF pulsations, which could result from magnetopause disturbances. Regardless, we already know there was a magnetopause disturbance from the THEMIS observations, and based on there being no evidence of a transient pressure pulse in the solar wind measured by either WIND or TH-B, a solar wind pressure pulse was likely not the cause of the event that occurred on 21 November 2008.

3.1.2.3. Hot Flow Anomaly

[18] On the basis of the characteristics of HFAs, we can further establish that the event was not the result of a HFA. Starting around the same time that the disturbance is first observed by TH-A, TH-D, and TH-E, hotter ion fluxes are measured by TH-B in Figure 4. These are likely diffuse back-streaming ions from the ion foreshock region [*Russell and Hoppe*, 1983] resulting from the IMF turning at ~1719:30 UT and TH-B being in the vicinity of the bow shock. The IMF-B_Y field discontinuity at ~1719:30 UT has no corresponding temperature spike, ion or electron flux enhancements, decrease in dynamic pressure, or change in the number density. However, the IMF discontinuity occurring at ~1730 UT could have resulted in either a foreshock cavity or a HFA around the time that TH-A first observed the event given the correct orientation of the discontinuity. TH-B observes this second IMF discontinuity around 9 min after the magnetopause disturbance is first observed by TH-A. Using the discontinuity normal direction calculated above from MVA and the $-\vec{V} \times \vec{B}$ electric field before and after the discontinuity (calculated with TH-B at 1729:00 and 1730:45 UT, respectively), we find that the electric field after the discontinuity passes is indeed directed back toward it, which is a necessary condition for HFA formation. Upon further analysis, there are several inconsistencies with previous works on HFAs. First, there is no plasma temperature spike observed by TH-B associated with this feature. Though the magnitude of the TH-B temperature data may be inaccurate due to the instrument being in the wrong mode, TH-B still observes very little variation in the temperature during the event. A temperature spike should be apparent independent of a magnitude offset. Next, there is no significant change in the solar wind velocity direction in either the ground-derived data (shown in Figure 4) or the spacecraft moment velocities (not shown here), which are available at higher time resolution. Also concerning the solar wind velocity, *Facsko et al.* [2008] found that fast solar wind speed is an essential condition for HFA formation. They found no HFAs for solar wind speeds less than 400 km/s, and for the event here, the solar wind speed is just under 300 km/s.

3.2. Fast Plasma Flows

[19] Concerning the plasma flows, TH-E observes the following velocity features upon encountering the initial magnetopause disturbance on 21 November 2008, V_N displaying a prolonged bipolar signature and a V_M signature that stays positive only through the center of the encounter. This strong, positive V_M encountered through the core of the disturbance is likely from the plasma moving through or with the event itself, and in the event that TH-E has simply crossed the magnetopause here, this velocity is that within the magnetosheath. Note that both TH-A and TH-E observe these fast, positive V_M flows (V_M > ~100 km/s) through most of the center of their respective encounters, but TH-D observes similar flows only very briefly. V_M is negative and V_L is positive on the flanks of the initial encounters by all three spacecraft, which reveal the fast magnetospheric flows around the disturbance itself. The dominant component of these magnetospheric flows as observed by TH-E is V_N, which is negative on the leading edge and strongly positive on the trailing edge of the initial disturbance. The negative V_M signatures indicate that the feature is moving faster than the ambient magnetospheric plasma [e.g., *Korotova et al.*, 2009], while the V_N signatures indicate it is displacing the magnetopause first inward then outward. Interestingly, these observations are consistent with the magnetospheric plasma flows around FTEs studied by *Liu et al.* [2008] and *Korotova et al.* [2009], and more discussion and interpretation of this follows in section 4.

[20] For TH-A and TH-D, which apparently do not cross fully into the event itself during their encounters, the velocity observations are somewhat different from TH-E. TH-D observes negative V_N flows before the event and positive V_N flows after it accompanied by a very clear tripolar signature in V_M. TH-A also observes a tripolar V_M signature. However, TH-A observes slightly positive V_N on the leading flank. These fast plasma flows are evidence of the magnetospheric plasma being forcefully diverted around the disturbance and are also manifested in the flux enhancements associated with the "wings" on either side of the disturbance in Figures 2b and 2c. The negative (positive) V_N signatures indicate inward (outward) motion of the magnetopause. V_M is also a strong component in these flows, and it is negative on the disturbance flanks, which is evidence that the event is mostly moving down the tail. Note too that all three spacecraft observe positive V_L signatures on at least one of the flanks of the disturbance (i.e., outside of the dashed lines in Figure 2). This indicates that the event is also moving in a slightly southward direction along the magnetopause.

[21] From Figure 2, the ion fluxes associated with these fast plasma flows are enhanced when compared to the fluxes at the same energies before and after the disturbance passes, and for the low-energy population, the magnitude of this enhancement and the energy at which it occurs are both correlated with the magnitude of the velocity of the flow. This is attributed to the cold plasma being heated as it is compressed ahead of and accelerated around the passing magnetopause disturbance. These "wings" are simply signatures of the magnetopause motion [e.g., *Sauvaud et al.*, 2001]. The $-\vec{V} \times \vec{B}$ electric field magnitude associated with the maximum velocity (as observed by TH-D) is calculated as 13.6 mV/m and is primarily in the negative M- and N-directions (the statistical magnetopause LMN components at 1721:55 UT are [0.9, −8.5, −10.6] mV/m). Similar

"wing" features are also evident in the electron distributions (see Figure 2).

[22] When pitch angle distributions are examined for the fast ion flows, they are not field-aligned, which is further proof that they are indeed plasma being displaced around the disturbance. Figure 6 shows the pitch angle flux spectrograms for TH-A, TH-D, and TH-E. Figure 6a is compiled of ion and electron fluxes from energy ranges corresponding to the cold plasma "wings," while Figure 6b is the same format but for energy ranges corresponding to the hot magnetospheric plasma. Using Figure 6a, we see that the lower-energy ions are perpendicular to the field and likely associated with plasma being displaced around the disturbance as it passes by the spacecraft. However, it is significantly different for the electrons featured here, which are field-aligned and bidirectional both just before and after each spacecraft encounters the disturbance. From Figure 6a, note that the peak fluxes of these field-aligned electrons are closest to the crossing boundary itself (i.e., between the white-dashed lines indicating the peaks in ion velocity, which are magnetospheric flows, and the disturbance itself, which has the highest low-energy ion and electron fluxes associated with it), and this is consistent with the idea that these are electrons residing along a separatrix layer that are remnants of some previous magnetic reconnection or ongoing reconnection along the boundary [e.g., *Owen et al.*, 2008]. From Figure 6b, it is apparent that there are also peaks in the higher energy fluxes corresponding to the peak ion velocities, and these peak fluxes consist of both electrons and ions with local pitch angles nearly perpendicular to the field. These too are magnetospheric plasma being diverted around the disturbance, but the pitch angle distributions for these higher energies are broader than those for the lower-energy plasma populations.

3.3. Density Enhancement

[23] Finally, we look at the density enhancement through the center of the initial magnetopause disturbance. TH-E observes the most significant density enhancement, which reaches a peak level of over 44 cm^{-3}. This is a factor of greater than 7X the near-Earth solar wind density as measured by TH-B (~6 cm^{-3}) and the upstream solar wind measured by WIND. In the magnetosheath, a density enhancement of 4X is expected across the subsolar bow shock based on the Rankine-Hugoniot jump conditions. However, TH-E is not near the subsolar bow shock, and according to the *Spreiter et al.* [1966] model, the sheath density near the magnetopause at ~0800 LT should only be a factor of ~2.5 times higher than that of the solar wind. The agreement between the TH-B ion densities corrected to the electron density when compared to those measured by WIND (see Figure 4) provides additional confidence in the accuracy of the solar wind density magnitude. Thus the event on 21 November 2008 reveals a compression of plasma density that, to our knowledge, has not yet been reported.

[24] The peaks in the ion density observed by TH-E occur around the start and stop times of the B_M rotational signature observed through the middle of the encounter (see period between the dash-dot-dotted lines in Figure 2). These maxima also roughly mark the start and stop times of the depression in the crater-like B_{Tot} observations. They occur just after the first peak in total pressure and just before the second peak is observed (the peaks in total pressure occur between the dash-dotted and dash-dot-dotted lines on either side of the disturbance in Figure 2). These peak locations are interesting in that they imply that there is a confined region of compressed plasma along some boundary of the disturbance itself. We speculate on this more in section 4. The density through the very center of TH-E's encounter actually dips to just over 20 cm^{-3}, which is more consistent with the expected magnetosheath plasma with the additional compression from the foreshock cavity features. Thus the density here also shows a crater-like feature, though over a different period than the crater-like feature in the total magnetic field strength.

[25] Concerning the peaks in total pressure, Figures 2g and 3e show the magnetic (green) and perpendicular thermal (red) pressures as well as their sum (black) through the event. Particularly evident in the TH-E data, the perpendicular thermal pressure becomes significantly stronger than the magnetic pressure through the core of the disturbance. The thermal pressure dominating over magnetic pressure through the core is consistent with TH-E going into sheath-like plasma. Also, the total pressure through the center of the disturbance observed by TH-E is not enhanced overall. However, at either edge of their encounters with the initial disturbance, TH-A and TH-E, observe local maxima in total pressure. The magnetic tension of the draped fields around the disturbance, the evidence of which is particularly clear in the B_M and B_N enhancements observed by all three spacecraft, must be recognized when considering any force balance through the event, and indeed these total pressure increases occur when the fields are most highly distorted based on their strong M- and N-components.

4. Discussion

[26] On the basis of the observations, we believe that TH-A and TH-D take glancing impacts from the initial magnetopause disturbance, while TH-E takes a direct impact and penetrates into the disturbance itself. TH-D probably does not encounter the event as closely as TH-A does based on the results from the pressure balance and the lack of a density enhancement. TH-A and TH-D encounter the dis-

Figure 6. (a) Pitch angle flux spectrograms for ions ranging from 10 to 1000 eV and electrons ranging from 10 to 500 eV, representing the lower-energy "wings." (b) Same as Figure 6a but for ions ranging from 1 to 20 keV and electrons ranging from 0.5 to 10 keV, representing the background magnetospheric plasma. For both Figures 6a and 6b, fluxes (units of eV/cm^2 s sr eV) are shown in color, and TH-A, TH-D, and TH-E results are shown from the top to the bottom with ion spectrograms appearing first and those for electrons appearing immediately below for each spacecraft. White dashed lines correspond to the times when the peak ion velocities (see Figure 2) are observed by each spacecraft both before and after the main disturbance is encountered. Note that the color scales for all plots are different here so as not to lose any information.

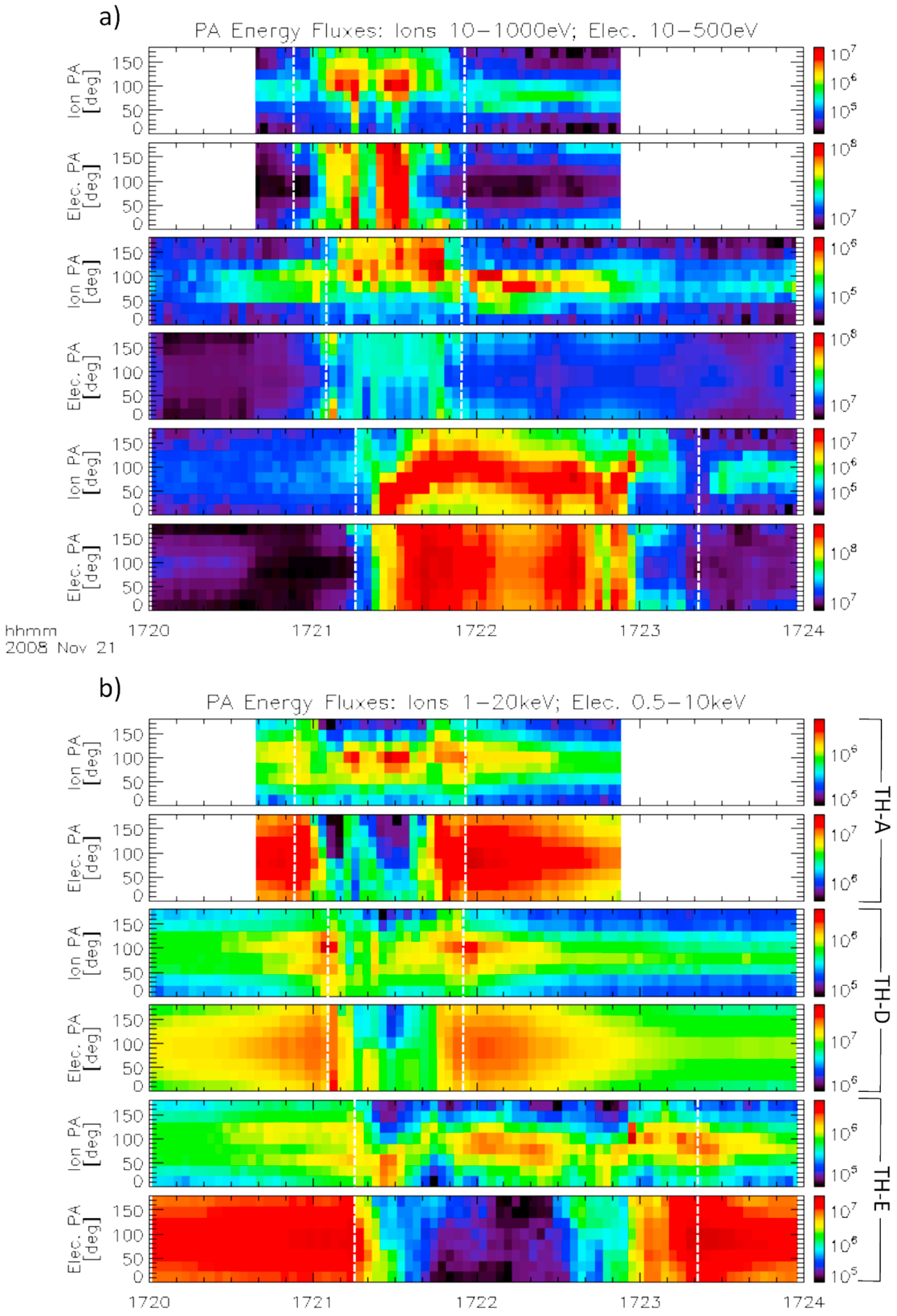
a)
PA Energy Fluxes: Ions 10–1000eV; Elec. 10–500eV
Ion PA [deg]
Elec. PA [deg]
150
100
50
0
hhmm
2008 Nov 21
1720
1721
1722
1723
1724
b)
PA Energy Fluxes: Ions 1–20keV; Elec. 0.5–10keV
TH-A
TH-D
TH-E

Figure 6

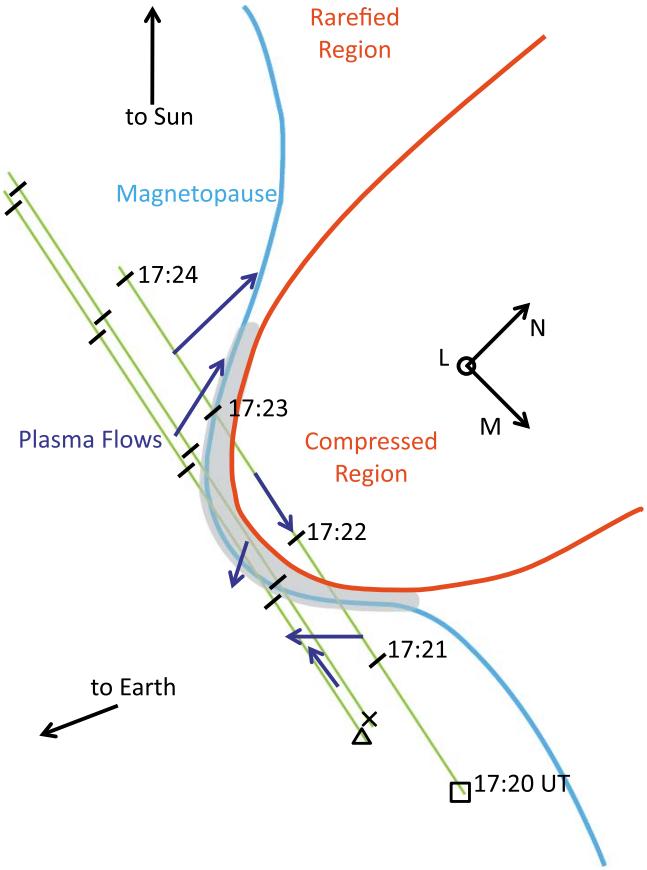

Figure 7. Sketch depicting a cross-section of the scenario in the M-N plane and moving with the event. TH-A (cross symbol), TH-D (triangle), and TH-E (square) are shown at 1720 UT with the same symbols as used for them as in Figure 1. Their estimated tracks through the event are shown with green lines and each minute after 1720 UT is marked with black bars and labeled along TH-E's track. The magnetopause boundary is shown with light blue and the leading-edge compression region of the foreshock cavity that resulted in the initial disturbance is shown with red. The shaded gray region represents the boundary region separating purely magnetospheric plasma and fields from those in the sheath. The rarefied density region of the foreshock cavity is also indicated, and the dark blue arrows approximate plasma flow magnitudes and directions as observed by the spacecraft before, during, and after the initial disturbance.

turbance first, and around 0.9 R_E down tail from TH-A, TH-E is the last to encounter it, which is consistent with the evidence that the event is moving tailward. TH-E makes clear measurements of the crater-type nature of the fields associated with this disturbance as well as the abnormal density enhancement along the boundaries of its core. After the initial disturbance, TH-E observes an overall enhancement followed by another depression in the total magnetic field strength and evidence from the plasma velocity that the magnetopause has moved outward and then back inward before returning to its preevent state. When the details of these observations are more closely examined, the large magnetopause disturbance observed by TH-A, TH-D, and TH-E on 21 November 2008 presents an intriguing scenario.

[27] The IMF discontinuity observed by TH-B at 1730 UT could have swept a foreshock cavity (either preexisting or generated by the discontinuity) along the magnetopause, which can explain many of the features observed by the three THEMIS spacecraft near the magnetopause. During the period from ~1719 to ~1730 UT, the IMF orientation is consistent with TH-B being located in the foreshock region (see Figure 5). Indeed, TH-B observes hot ions that are characteristic of the foreshock from ~1721 to ~1730 UT, when the IMF discontinuity occurs. Between ~1728 and ~1731 UT, TH-B observes crater-like features in the total field strength, plasma density, and dynamic pressure, which are characteristic features consistent with both theory [*Thomas and Brecht*, 1988] and observations [e.g., *Sibeck et al.*, 2002] of foreshock cavities upstream of the bow shock. Given the results of a minimum variance analysis on the IMF discontinuity at 1730 UT, the solar wind velocity, and our current understanding of foreshock cavities, the effects of a foreshock cavity moving with the discontinuity could have propagated through the sheath and been observed by TH-A, TH-D, and TH-E starting shortly before 1721 UT.

[28] Concerning the observations of the initial disturbance at the magnetopause resulting from the leading-edge compressed region of the foreshock cavity, Figure 7 is a simplified picture of the initial disturbance that explains many of the features observed by TH-A, TH-D, and TH-E during their encounters from 1720 to 1724 UT. Figure 7 shows a basic sketch depicting a cross-section of the scenario in the M-N plane, and it can be used as a visual reference for the following discussion on what TH-A, TH-D, and TH-E observed as they each encountered different parts of this disturbance. Starting with TH-D (shown by a triangle symbol) in Figure 7, the spacecraft observes the clearest plasma flow signatures (represented before, during, and after the initial disturbance by dark blue arrows in Figure 7) and apparently just barely penetrates into the boundary layer (shaded gray region), which includes the low-latitude boundary layer (LLBL) as shown here and is apparently the transition region between purely magnetospheric plasmas and those in the disturbance. The magnetic fields around the event must also be distorted to have stronger M and N components, which TH-D also observes and is consistent with the TH-A and TH-E observations when they are also in this boundary layer. TH-A (cross symbol in Figure 7) makes similar observations to TH-D though apparently skirts closer to the edge of the disturbance. Unlike TH-D and TH-E when they first encounter the event, TH-A observes slightly positive V_N flow, which may be a result of vorticity in the flows along the boundary. We propose that TH-A never fully enters into the disturbance since it does not observe a reversal in the B_M component or the intense density enhancement like TH-E, though it probably gets close based on the similarity to the TH-E total velocity, flux, density, temperature, and pressure observations in Figure 2.

[29] The picture in Figure 7 is also useful in explaining many of the features observed by TH-E (shown by a square symbol) between 1720 and 1724. The fields and velocities measured by TH-E through its encounter indicate three distinct plasma regions during this time period:

the magnetospheric plasma flowing around the event, a complex boundary layer, and the magnetosheath plasma. As the spacecraft begins to encounter the magnetopause disturbance, it observes fast plasma flows that are primarily in the negative N-direction. Also just as it starts to encounter the disturbance, TH-E observes a positive V_L in the magnetospheric flows indicating that the event is moving with a slight negative V_L component. Meanwhile, the V_M component is negative, which is consistent with the other spacecraft observations and is evidence of the event moving tailward. Upon entering the boundary layer, TH-E observes the distorted magnetospheric and sheath fields, with enhanced M- and N-components and a significantly weak L-component. In Figure 2, TH-E would be passing through this boundary layer during the periods between the dash-dotted and dash-dot-dotted lines. Going fully through the boundary layer, the spacecraft sees a reversal in the M-component of the field, which along with the depleted hot plasma is indicative of entering a new plasma region. It is at the transition between the boundary layer and compressed region, as indicated by the dash-dot-dotted lines in Figure 2, that TH-E observes the abnormally strong peaks in the plasma density. Upon exiting the disturbance again through the boundary layer and into purely magnetospheric field, TH-E again observes the draped magnetospheric fields with their positive B_M and negative B_N components. After TH-E has passed through the event shortly after 1723 UT, it encounters the fast magnetospheric plasma flows being diverted around the disturbance, and these flows display a very strong positive V_N-component, which are evidence of the magnetospheric plasma rushing very rapidly outwards after the initial disturbance has passed. These strong flows are consistent with this event being a foreshock cavity being swept over the magnetopause by an IMF discontinuity. After the initial compression region flanking the cavity passes by TH-E, the magnetopause, which was pushed inward over TH-E during the initial compression, would push back outward rapidly in response to the depressed densities through the cavity itself.

[30] In the magnetosheath, this foreshock cavity is apparently asymmetric concerning the intensity of its compressed edges; the compression region on the leading edge is more intense than that on the trailing edge. From TH-E, the initial compression region (i.e., on the event's leading edge) is encountered from ~1721 to 1723. During this part of the event, the magnetopause is moved inward over TH-A, TH-D, and TH-E. TH-A and TH-D apparently never leave a boundary layer between the magnetosphere and pure sheath plasmas, but TH-E apparently penetrates through the boundary layer and into the compressed region in the sheath, which exhibits an overall enhancement in plasma density above 20 cm^{-3}. The density cavity region, which results in the magnetopause initially moving back radially outward, is encountered by TH-E from ~1723 to 1726, and the trailing compression region is apparently encountered from ~1726 to 1728. This second compression region does not result in any of the three magnetospheric THEMIS spacecraft from entering into the sheath, though TH-E apparently gets close to the magnetopause again based on the observations seen in Figure 3 (note the enhanced fluxes, drop in total field strength, enhanced velocities, and pressures, which are comparable to when TH-E is near the boundary during the initial disturbance). Additionally, the slightly southward and strong tailward motion of the event as observed by TH-A, TH-D, and TH-E is consistent with how a foreshock cavity moving with the IMF current sheet would be swept along the magnetopause.

[31] Interestingly, several of the features associated with this event are similar to those of other magnetopause phenomena. The fast flows around the initial disturbance resulting from the leading compression region are very similar to the plasma flows around FTEs described by *Liu et al.* [2008] and *Korotova et al.* [2009]. Also, the crater-like signature in the total magnetic field observed by TH-E is similar to those for crater-type FTEs [e.g., *Zhang et al.*, 2010]. Indeed, there is evidence of reconnection along the event boundary in the form of the field-aligned electrons, and *Jacob and Cattell* [1993] discussed how IMF discontinuities in which B_Z turns from southward to northward might be a favorable condition for FTE generation. However, the lack of a continuous bipolar B_N signature is strong evidence against the full disturbance resulting from a FTE. The inward-outward-inward magnetopause motion observed by TH-E could be mistaken for boundary waves associated with the KH instability. Similar to magnetopause motion resulting from transient pressure pulses in the solar wind [e.g., *Sibeck*, 1990, 1992], MIEs are observed. However, MIEs should be signatures of any phenomena resulting in magnetopause motion [*Glassmeier*, 1992]. By their nature, foreshock cavities and HFAs have many similar features, though for the event in question here, there is no temperature spike or flow reversal at TH-B, which would be distinct evidence of a HFA. Most recently, *Omidi et al.* [2010] introduced a new foreshock phenomena they called foreshock bubbles. On the basis of their simulations, foreshock bubbles are associated with IMF discontinuities and should generate similar features to foreshock cavities as observed by in situ spacecraft. However, to determine if the conditions on 21 November 2008 were appropriate for the generation of a foreshock bubble, global simulations are necessary, which are beyond the scope of this observational report.

[32] Concerning the TH-E observations of the extreme density enhancement associated with this event, the combined factors of the enhanced density in the magnetosheath itself (i.e., a factor of ~2.5 times the solar wind density based on the *Spreiter et al.* [1966] model) along with the enhanced densities at the edges of a foreshock cavity may explain the density of more than 20 cm^{-3} observed by TH-E in the pure sheath plasma. Sheath density enhancements in the bounding compression regions of foreshock cavities were reported previously by *Sibeck et al.* [2000], but to our knowledge, the magnitude of the compression reported here, i.e., >7X the density of the nearby solar wind, has not been previously reported. Furthermore, it seems as though the highest enhanced plasma densities associated with this foreshock cavity are compressed against the boundary layer itself, with its enhanced total pressure and distorted magnetic fields between the compressed region and the magnetopause. These confined peaks in density of over 44 cm^{-3} along the boundary layer imply some additional localized compression mechanism. This is evidence of some complex behavior in this boundary layer that apparently further magnifies the density enhancement from 20 cm^{-3} to more than 44 cm^{-3}. If this is indeed the case,

it introduces some interesting questions. Why are the strongest density enhancements restricted spatially to near the boundary layer? What process in this boundary layer results in the additional compression? How strong can such a density enhancement get? The most direct way to address these questions is with detailed numerical simulations [e.g., *Omidi and Sibeck*, 2007] using spacecraft observations, like those presented here, for input and validation.

5. Conclusions

[33] The magnetopause disturbance observed by three of the THEMIS spacecraft on 21 November 2008 presents a complex yet interesting case with several clear and detailed features. In this observational report, we have presented the evidence and propose that the most likely explanation of this event is a foreshock cavity, the effects of which propagated into the sheath and impinged upon the magnetopause. Additionally, this foreshock cavity was apparently swept along the bow shock by a tangential discontinuity in the IMF. If this is indeed the case, it is additional observational evidence in support of the conceptual model of such a case presented by *Sibeck et al.* [2000]. This foreshock cavity was also asymmetric as observed by TH-E, with the compression region on its leading edge being stronger than the trailing compression region. We find that the scale size in the direction of the event's velocity was ~8 R_E, both in the sheath along the magnetopause and at TH-B's location in the solar wind near the bow shock, which is interesting given the spatial separation between the two spacecraft. However, the intensity of the event's features was weaker as observed by TH-B, which is consistent with previous works on foreshock cavities [e.g., *Sibeck et al.*, 2004]. Also, the size of the leading edge compression region along the magnetopause is ~1 R_E.

[34] We have gone into detail analyzing the fast magnetospheric plasma flows encountered around the initial disturbance, and we find that the fast ion flows are mostly perpendicular to the field and are the result of plasma being displaced around the disturbance itself as it moved along the magnetopause. Interestingly, these flows are comparable to those for FTEs studied by *Liu et al.* [2008] and *Korotova et al.* [2009]. This demonstrates that the magnetospheric flows around transient magnetopause disturbances resulting from different phenomena can be similar. Here we have also analyzed the pitch angle flux spectrograms associated with these flows. The "wing" signatures in the ion flux distributions are simply evidence of the magnetopause motion. The low-energy electrons associated with the highest-speed electron flows are field-aligned, unlike their ion counterparts, and are consistent with separatrix-layer electrons that are associated with reconnection [e.g., *Owen et al.*, 2008].

[35] In addition to these fast plasma flows and clear "wings" in the plasma flux distributions, the initial disturbance displays an abnormal compression of plasma density throughout its central core of over 20 cm^{-3} including confined regions along the boundary layer of over 44 cm^{-3}, which is more than 7 times the density of the near-Earth solar wind and is significantly higher than the factor of 4 expected in the subsolar magnetosheath from the Rankine-Hugoniot jump conditions across the bow shock. We conclude that this is most likely an extreme density enhancement resulting from the foreshock cavity event, perhaps resulting from a combination of compression effects due to the magnetosheath and the cavity's leading-flank compression region coupled with some additional compression due to complex interactions near the magnetopause along the event's boundary layer. This density enhancement and the detailed and asymmetric features associated with this foreshock cavity event are intriguing, and we propose that these multipoint THEMIS observations from the magnetosphere, sheath, and near-bow shock solar wind on 21 November 2008 should prove useful for detailed reconstruction and simulations of this event, which may prove to be particularly beneficial to our understanding of magnetopause disturbances and the complex nature of solar wind-magnetosphere interactions.

[36] **Acknowledgments.** We would first like to thank the reviewers for their useful comments, which have proven very beneficial to this work. The authors thank the THEMIS team for its online data access and IDL toolset, which have proven invaluable to this study. We also thank R. Lin, K. Ogilvie, and H. Singer for providing data for NASA's CDAWeb database and the TIPSOD 4-D Orbit Viewer team from NASA. D. L. Turner would like to personally thank D. G. Sibeck, R. C. Fear, J. P. McCollough, and L. Andersson for insightful discussions. This work was supported by NSF grants (ATM-0902813). K. H. Glassmeier acknowledges financial support by the German Ministerium für Wirtschaft und Technologie and the Deutsches Zentrum für Luft- und Raumfahrt under grant 50QP0402.

[37] Robert Lysak thanks Robert Fear and another reviewer for their assistance in evaluating this paper.

References

Angelopoulos, V. (2008), The THEMIS mission, *Space Sci. Rev.*, *141*, doi:10.1007/s11214-008-9336-1.

Auster, H. U., K. H. Glassmeier, W. Magnes, O. Aydogar, W. Baumjohann, D. Constantinescu, D. Fischer, K. H. Fornacon, E. Georgescu, and P. Harvey (2008), The THEMIS fluxgate magnetometer, *Space Sci. Rev.*, *141*, 235–264, doi:10.1007/s11214-008-9365-9.

Billingham, L., S. J. Schwartz, and D. G. Sibeck (2008), The statistics of foreshock cavities: Results of a Cluster survey, *Ann. Geophys.*, *26*, 3653–3667, doi:10.5194/angeo-26-3653-2008.

Facsko, G., K. Kecskemety, G. Erdos, M. Tatrallyay, P. W. Daly, and I. Dandouras (2008), A statistical study of hot flow anomalies using Cluster data, *Adv. Space Res.*, *41*(8), 1286–1291, doi:10.1016/j.asr.2008.02.005.

Fairfield, D. H. (1971), Average and unusual locations of the Earth's magnetopause and bow shock, *J. Geophys. Res.*, *76*, 6700–6716, doi:10.1029/JA076i028p06700.

Fairfield, D. H., W. Baumjohann, G. Paschmann, H. Luhr, and D. G. Sibeck (1990), Upstream pressure variations associated with the bow shock and their effects on the magnetosphere, *J. Geophys. Res.*, *95*, 3773–3786, doi:10.1029/JA095iA04p03773.

Glassmeier, K. H. (1992), Traveling magnetospheric convection twin vortices—Observations and theory, *Ann. Geophys.*, *10*, 547–565.

Hasegawa, H., M. Fujimoto, T.-D. Phan, H. Reme, A. Balogh, M. W. Dunlop, C. Hashimoto, and R. TanDokoro (2004), Transport of solar wind into Earth's magnetosphere through rolled up Kelvin-Helmholtz vortices, *Nature*, *430*, 755–758, doi:10.1038/nature02799.

Jacob, J. D., and C. Cattell (1993), High-time resolution measurements of upstream magnetic field and plasma conditions during flux transfer events at the Earth's dayside magnetopause, *Geophys. Res. Lett.*, *20*, 2007–2010, doi:10.1029/93GL00845.

Jacobsen, K. S., et al. (2009), THEMIS observation of extreme magnetopause motion caused by a hot flow anomaly, *J. Geophys. Res.*, *114*, A08210, doi:10.1029/2008JA013873.

Korotova, G. I., D. G. Sibeck, and T. Rosenberg (2009), Geotail observations of FTE velocities, *Ann. Geophys.*, *27*, 83–92, doi:10.5194/angeo-27-83-2009.

Liu, J., V. Angelopoulos, D. Sibeck, T. Phan, Z. Y. Pu, J. McFadden, K. H. Glassmeier, and H. U. Auster (2008), THEMIS observations of the dayside traveling compression region and flows surrounding flux transfer events, *Geophys. Res. Lett.*, *35*, L17S07, doi:10.1029/2008GL033673.

McFadden, J. P., C. W. Carlson, D. Larson, V. Angelopoulos, M. Ludlam, R. Abiad, B. Elliott, P. Turin, and M. Marckwordt (2008), The THEMIS

ESA plasma instrument and in-flight calibration, *Space Sci. Rev.*, *141*, 277–302, doi:10.1007/s11214-008-9440-2.

Omidi, N., and D. G. Sibeck (2007), Flux transfer events in the cusp, *Geophys. Res. Lett.*, *34*, L04106, doi:10.1029/2006GL028698.

Omidi, N., J. P. Eastwood, and D. G. Sibeck (2010), Foreshock bubbles and their global magnetospheric impacts, *J. Geophys. Res.*, *115*, A06204, doi:10.1029/2009JA014828.

Otto, A., and D. H. Fairfield (2000), Kelvin-Helmholtz instability at the magnetotail boundary: MHD simulations and comparison with Geotail observations, *J. Geophys. Res.*, *105*, 21,175–21,193, doi:10.1029/1999JA000312.

Owen, C. J., A. Marchaudon, M. W. Dunlop, A. N. Fazakerley, J.-M. Bosqued, J. P. Dewhurst, R. C. Fear, S. A. Fuselier, A. Balogh, and H. Reme (2008), Cluster observations of "crater" flux transfer events at the dayside high-latitude magnetopause, *J. Geophys. Res.*, *113*, A07S04, doi:10.1029/2007JA012701.

Russell, C. T., and M. M. Hoppe (1983), Upstream waves and particles, *Space Sci. Rev.*, *34*, 155–172, doi:10.1007/BF00194624.

Russell, C. T., and R. C. Elphic (1978), Initial ISEE magnetometer results: Magnetopause observations, *Space Sci. Rev.*, *22*, 681–715, doi:10.1007/BF00212619.

Sauvaud, J.-A., et al. (2001), Intermittent thermal plasma acceleration linked to sporadic motions of the magnetopause, first Cluster results, *Ann. Geophys.*, *19*, 1523–1532.

Schwartz, S. J., et al. (1985), An active current sheet in the solar wind, *Nature*, *318*, 269–271.

Schwartz, S. J., D. Sibeck, M. Wilber, K. Meziane, and T. S. Horbury (2006), Kinetic aspects of foreshock cavities, *Geophys. Res. Lett.*, *33*, L12103, doi:10.1029/2005GL025612.

Shue, J.-H., J. K. Chao, H. C. Fu, C. T. Russell, P. Song, K. K. Khurana, and H. J. Singer (1997), A new functional form to study the solar wind control of the magnetopause size and shape, *J. Geophys. Res.*, *102*, 9497–9511, doi:10.1029/97JA00196.

Sibeck, D. G. (1990), A model for the transient magnetospheric response to sudden solar wind dynamic pressure variations, *J. Geophys. Res.*, *95*, 3755–3771, doi:10.1029/JA095iA04p03755.

Sibeck, D. G. (1992), Transient events in the outer magnetosphere: Boundary waves or flux transfer events?, *J. Geophys. Res.*, *97*, 4009–4026, doi:10.1029/91JA03017.

Sibeck, D. G., et al. (1989), The magnetospheric response to 8-minute period strong-amplitude upstream pressure variations, *J. Geophys. Res.*, *94*, 2505–2519, doi:10.1029/JA094iA03p02505.

Sibeck, D. G., et al. (2000), Magnetopause motion driven by interplanetary magnetic field variations, *J. Geophys. Res.*, *105*, 25,155–25,169, doi:10.1029/2000JA900109.

Sibeck, D. G., R. B. Decker, D. G. Mitchell, A. J. Lazarus, R. P. Lepping, and A. Szabo (2001), Solar wind preconditioning in the flank foreshock: IMP 8 observations, *J. Geophys. Res.*, *106*, 21,675–21,688, doi:10.1029/2000JA000417.

Sibeck, D. G., T.-D. Phan, R. Lin, R. P. Lepping, and A. Szabo (2002), Wind observations of foreshock cavities: A case study, *J. Geophys. Res.*, *107*(A10), 1271, doi:10.1029/2001JA007539.

Sibeck, D. G., K. Kudela, T. Mukai, Z. Nemecek, and J. Safrankova (2004), Radial dependence of foreshock cavities: A case study, *Ann. Geogr.*, *22*, 4143–4151.

Sonnerup, B. U. O., and M. Scheible (1998), Minimum and maximum variance analysis, in *Analysis Methods for Multi-Spacecraft Data*, *ISSI Sci. Rep. SR-001*, edited by G. Paschmann and P. W. Daly, pp. 185–220, Eur. Space Agency Publ. Div., Noordwijk, Netherlands.

Spreiter, J. R., A. L. Summers, and A. Y. Alksne (1966), Hydromagnetic flow around the magnetosphere, *Planet. Space Sci.*, *14*, 223–253, doi:10.1016/0032-0633(66)90124-3.

Thomas, V. A., and S. H. Brecht (1988), Evolution of diamagnetic cavities in the solar wind, *J. Geophys. Res.*, *93*, 11,341–11,353, doi:10.1029/JA093iA10p11341.

Thomsen, M. F., J. T. Gosling, S. A. Fuselier, S. J. Bame, and C. T. Russell (1986), Hot, diamagnetic cavities upstream from the Earth's bow shock, *J. Geophys. Res.*, *91*, 2961–2973, doi:10.1029/JA091iA03p02961.

Thomsen, M. F., V. A. Thomas, D. Winske, J. T. Gosling, M. H. Farris, and C. T. Russell (1993), Observational test of hot flow anomaly formation by the interaction of a magnetic discontinuity with the bow shock, *J. Geophys. Res.*, *98*, 15,319–15,330, doi:10.1029/93JA00792.

Zhang, H., et al. (2010), Evidence that crater FTEs are initial stages of typical FTEs, *J. Geophys. Res.*, *115*, A08229, doi:10.1029/2009JA015013.

V. Angelopoulos, Department of Earth and Space Sciences, University of California, Los Angeles, CA 90095, USA.

S. Eriksson, W. Liu, and W.-L. Teh, Laboratory for Atmospheric and Space Physics, University of Colorado at Boulder, Boulder, CO 80309, USA.

K.-H. Glassmeier, Institut für Geophysik and Extraterrestrische Physik, Technische Universität Braunschweig, Mendelssohnstr. 3, Braunschweig D-38106, Germany.

X. Li, W. Tu, and D. L. Turner, Department of Aerospace Engineering Sciences, University of Colorado at Boulder, Boulder, CO 80309, USA. (drew.lawson.turner@gmail.com)

J. P. McFadden and T. D. Phan, Space Sciences Laboratory, University of California, Berkeley, CA 94720, USA.